Engineering 28 (2023) 49–57

Contents lists available at ScienceDirect

Engineering

journal homepage: www.elsevier.com/locate/eng

Research
Space-Deployable Structure—Article

A Shape-Memory Deployable Subsystem with a Large Folding Ratio in China's Tianwen-1 Mars Exploration Mission

Chengjun Zeng [a], Liwu Liu [a], Yang Du [b], Miao Yu [b], Xiaozhou Xin [a], Tianzhen Liu [c], Peilei Xu [a], Yu Yan [a], Dou Zhang [a], Wenxu Dai [a], Xin Lan [c], Fenghua Zhang [c], Linlin Wang [c], Xue Wan [c], Wenfeng Bian [d], Yanju Liu [a,*], Jinsong Leng [c,*]

[a] Department of Astronautical Science and Mechanics, Harbin Institute of Technology, Harbin 150001, China
[b] Shanghai Institute of Satellite Engineering, Shanghai 201109, China
[c] Center for Composite Materials and Structures, Harbin Institute of Technology, Harbin 150080, China
[d] Department of Civil Engineering, Harbin Institute of Technology, Weihai 264209, China

ARTICLE INFO

Article history:
Received 3 May 2022
Revised 29 October 2022
Accepted 13 January 2023
Available online 1 March 2023

Keywords:
Flexible deployable structure
Shape memory polymer composite
Mars exploration
Temperature telemetry
On-orbit deployment

ABSTRACT

Once China's Tianwen-1 Mars probe arrived in a Mars orbit after a seven-month flight in the deep cold space environment, it would be urgently necessary to monitor its state and the surrounding environment. To address this issue, we developed a flexible deployable subsystem based on shape memory polymer composites (SMPC-FDS) with a large folding ratio, which incorporates a camera and two temperature telemetry points for monitoring the local state of the Mars orbiter and the deep space environment. Here, we report on the development, testing, and successful application of the SMPC-FDS. Before reaching its Mars remote-sensing orbit, the SMPC-FDS is designed to be in a folded state with high stiffness; after reaching orbit, it is in a deployed state with a large envelope. The transition from the folded state to the deployed state is achieved by electrically heating the shape memory polymer composites (SMPCs); during this process, the camera on the SMPC-FDS can capture the local state of the orbiter from multiple angles. Moreover, temperature telemetry points on the SMPC-FDS provide feedback on the environment temperature and the temperature change of the SMPCs during the energization process. By simulating a Mars on-orbit space environment, the engineering reliability of the SMPC-FDS was comprehensively verified in terms of the material properties, structural dynamic performance, and thermal vacuum deployment feasibility. Since the launch of Tianwen-1 on 23 July 2020, scientific data on the temperature environment around Tianwen-1 has been successfully acquired from the telemetry points on the SMPC-FDS, and the local state of the orbiter has been photographed in orbit, showing the national flag of China fixed on the orbiter.

1. Introduction

Within the constraints of limited mass and compact space, the rapid development of deep space exploration has posed demanding challenges in terms of the materials and structural technology of the probe payload [1]. Large payloads on the probe, such as solar sails, antennas, radars, and sunshades, are usually designed as deployable mechanisms to save space during the launch and flight [2,3]. These deployable mechanisms are required to be as lightweight as possible and must exhibit satisfactory stability during deployment [4,5]. Recently, the emergence of flexible deployable structures based on smart soft materials has addressed these challenges [6,7].

Shape memory polymers (SMPs) are typically smart soft materials that can transform from a temporary configuration back into their original configuration in response to specific external stimuli such as heat, light, electricity, magnetism, or a solution [8–14]. Their velocity-controlled shape-transformation process makes SMPs attractive for use in mechanically sensitive deployable structures for spacecraft. Shape memory polymer composites (SMPCs) combine the ultra-light weight, large deformability, and variable stiffness of SMPs with the high stiffness/strength of reinforcing

* Corresponding authors.
E-mail addresses: yj_liu@hit.edu.cn (Y. Liu), lengjs@hit.edu.cn (J. Leng).

https://doi.org/10.1016/j.eng.2023.01.005

materials such as carbon fibers, resulting in significantly better specific stiffness/strength and deformability than those of traditional metallic materials such as shape memory alloys [15–17]. SMPCs overcome the shortcomings of pure SMPs, which include a low modulus and low recovery force, and thus provide a viable solution for flexible deployable structures that can be used in deep space exploration. A variety of flexible deployable structures based on SMPCs have been developed, such as shape-memory hinges [18], extendible booms [19], and deployable antennas [20]. Among these, shape-memory hinges, as simple flexible units, can be used to form complex deployable structures such as solar sails and trusses via multi-stage assembly [21,22]. Furthermore, several SMPC-based flexible deployable structures have been qualified by spatial proof-of-principle demonstrations and have been preliminarily applied. For example, an SMPC-based sunlight-stimulated substrate successfully underwent deployment experiments and anti-irradiation validation on a geostationary satellite orbit in 2016 [23]. In 2020, the world's first aerospace on-orbit demonstration of an SMPC-based flexible solar array was reported [24]. These successful space-principle demonstrations show the promise of SMPC-based flexible deployable structures for deep space exploration.

Tianwen-1, which was successfully launched on 23 July 2020, is China's first independent Mars exploration mission; it consists of an orbiter, lander, and rover [25,26]. According to the overall requirements of the Tianwen-1 mission, the local state of the orbiter and its surrounding environment require monitoring. However, the space of the orbiter is occupied by seven effective scientific instruments, so the issue of how to accomplish this task presented a technical challenge to the design team [27]. To address this challenge, we designed a flexible deployable subsystem based on SMPC (SMPC-FDS), which consists of a lock–release mechanism and a multi-stage deployable mechanism.

Before the orbiter reaches a Mars remote-sensing orbit, the multi-stage deployable mechanism is in a folded state and locked by the lock–release mechanism, so the entire SMPC-FDS is in a compact state with high rigidity and a small envelope. After reaching the Mars remote-sensing orbit, the lock–release mechanism is unlocked by the SMPCs and releases the multi-stage deployable mechanism. This mechanism is then driven by SMPC hinges to deploy into a straight rod with a length of 1.6 m; then, the camera at the end of the straight rod can capture the local state of the orbiter. In addition, two temperature telemetry points are respectively arranged on the lock–release mechanism and the multi-stage deployable mechanism to enable real-time monitoring of the space environment around the orbiter. A series of ground qualification experiments such as tensile tests, dynamic mechanical analysis, structural shock/vibration tests, and thermal vacuum deployment tests were performed to validate the engineering safety and deployment reliability of the SMPC-FDS. Since the launch of Tianwen-1, scientific data on the deep space environment around the orbiter has been continuously obtained from the temperature telemetry points of the SMPC-FDS. Moreover, the SMPC-FDS was successfully deployed in a Mars remote-sensing orbit on 11 November 2021, to assist the associated camera in scientific photography missions.

2. Materials and methods

2.1. Design of the SMPC-FDS

As shown in Fig. 1(a), Tianwen-1 has gone through six phases from launch to a Mars remote-sensing orbit: ① the launch phase, ② the Earth–Mars transfer phase, ③ the Mars capture phase, ④ the Mars mooring phase, ⑤ the relay communication phase, and ⑥ the remote-sensing phase [28]. To adapt to the harsh space environment and the unpredictable mechanical environment caused by multiple reorbits during this flight, the SMPC-FDS is in a folded state, mounted in the $+Y$–Z quadrant of the orbiter, as shown in Fig. 1(b). The SMPC-FDS consists of a lock–release mechanism with a double locking function and a multi-stage deployable mechanism composed of multiple SMPC hinges connected in series, whose unlocking and deploying functions depend on the shape memory effect of the SMPCs. The functional components of the lock–release mechanism are SMPC-based locking and releasing laminates, while the key components of the multi-stage deployable mechanism are four SMPC hinges. Details on the structural design of the SMPC-FDS are provided in Fig. S1 in Appendix A.

In the folded state, the field of view of the camera on the SMPC-FDS is below the front of the orbiter, so the orbiter itself and the national flag of China fixed on the orbiter cannot be photographed. When Tianwen-1 enters its Mars remote-sensing orbit, the scientific mission of monitoring the local state of the orbiter must be executed. The lock–release mechanism first unlocks and releases the multi-stage deployable mechanism under telemetry control, followed by the graded deployment of SMPC hinges in the multi-stage deployable mechanism. The final deployed SMPC-FDS is shown in Fig. 1(c). In the SMPC-FDS's deployed state, the camera's field of view faces the orbiter; the national flag of China is located in the center of the camera's field of view, so the local state of the orbiter can be photographed and transmitted back to Earth. Schematic diagrams for the unlocking and deploying process of the SMPC-FDS are detailed in Fig. S1. Fig. 1(d) presents a physical view of the SMPC-FDS on Tianwen-1. Based on the given design scheme, two additional temperature telemetry points (whose locations are shown in Fig. 1(e)) are arranged on the SMPC-FDS; these can not only monitor the space environment temperature during the flight of Tianwen-1 but also provide feedback on the temperature changes of the SMPC releasing laminate in the lock–release mechanism and the first hinge in the multi-stage deployable mechanism during the deployment process.

2.2. Materials and fabrication

The functional components of the SMPC-FDS are one cyanate-based SMPC (CSMPC) locking laminate, two CSMPC releasing laminates, and four epoxy-based SMPC (ESMPC) hinges. The CSMPC has a high glass transition temperature (T_g) of over 170 °C and high mechanical strength, which structurally enhances the stiffness of the SMPC-FDS in the folded state. In comparison, the ESMPC possesses a low T_g of less than 150 °C, which improves the deployment reliability of the SMPC-FDS in the case of limited power being provided by the orbiter. The respective SMPs used to fabricate the CSMPC and ESMPC are a thermosetting cyanate-based SMP and an epoxy-based SMP synthesized by Prof. Jinsong Leng's team at Harbin Institute of Technology, China; both SMPs possess excellent shape memory performance and temperature-induced variable stiffness capability [29–31]. The reinforcement material is a Toray T300-3 K plain-weave fabric with a fiber lay-up direction of ±45°, and the material fabrication process is vacuum-assisted resin transfer molding (VARTM) [32].

The design and physical drawings of the SMPC hinge in the folded and deployed states are respectively provided in Figs. S2(a) and (b) in Appendix A. The original shape of the SMPC hinge is straight; a load is applied at 150 °C to bend it by nearly 180°, which is followed by a reduction in temperature to room temperature to fix the temporary shape. When activated by high temperature, the SMPC sheet automatically recovers from the temporary shape to its original shape. Fig. S2(c) in Appendix A presents a schematic diagram of the SMPC-based lock–release mechanism in the locking and releasing states. The locking laminate and the releasing laminate function similarly to the SMPC hinge. The temporary

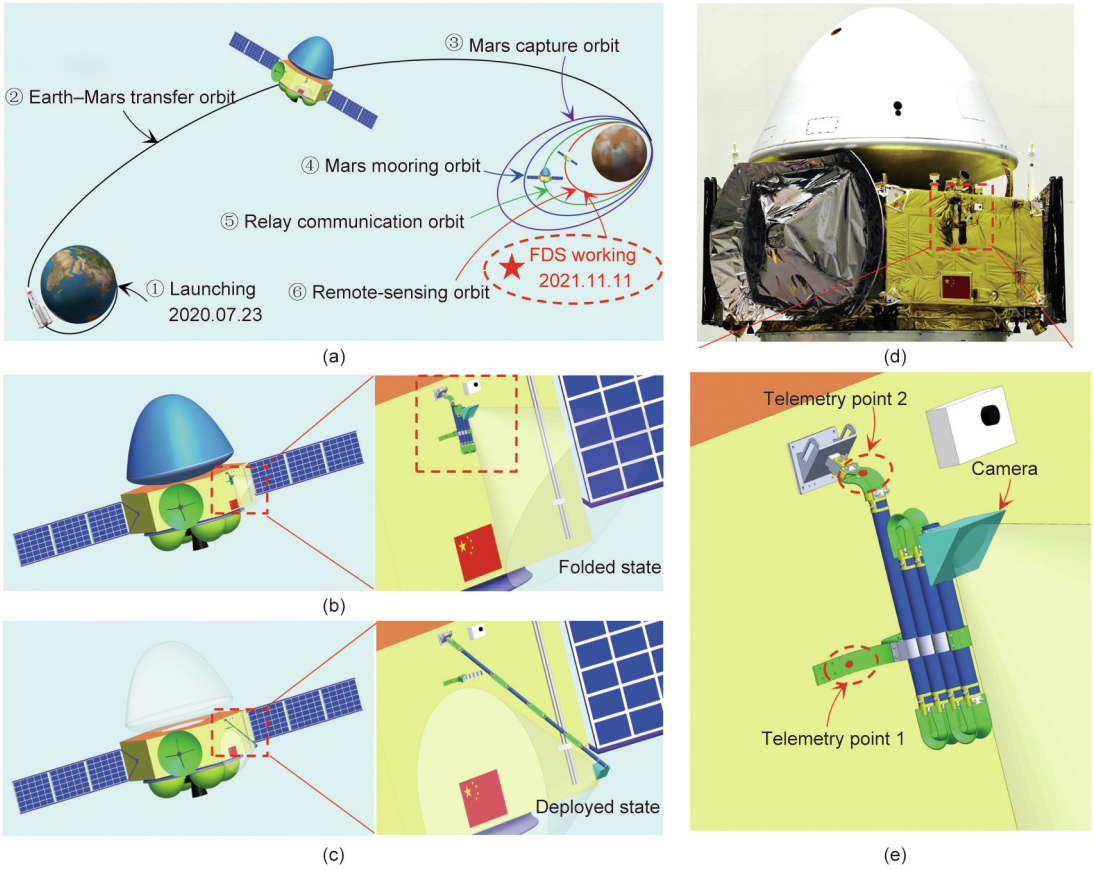

Fig. 1. The flight trajectory of the SMPC-FDS on Tianwen-1 and its structural design. (a) The whole flight trajectory of the SMPC-FDS; (b) schematic diagram of the SMPC-FDS in its folded state; (c) schematic diagram of the SMPC-FDS in its deployed state; (d) physical view of the SMPC-FDS on the Tianwen-1 probe; (e) arrangement of the two temperature telemetry points on the SMPC-FDS.

and original shapes of the locking laminate are curved and straight, respectively; the original and temporary shapes of the releasing laminate are respectively shown in the right and left diagrams of Fig. S2(c). Fig. S2(d) in Appendix A provides physical views of the locking laminate and the releasing laminate.

It is a challenge to heat the SMPC laminates (including the hinge, locking laminate, and releasing laminate) in order to deploy them automatically when the SMPC-FDS is in a Mars orbit far from Earth. Fortunately, Lan et al. [24] proposed a method for heating an SMPC laminate using a flexible film-type electric heater and verified the feasibility of the method. In this work, this heating method was adopted. As shown in Fig. S2(e) in Appendix A, a layer of polyimide double-sided pressure-sensitive tape (PI013-ST; Beijing Tianyu Aerospace New Material Technology Co., Ltd., China) was first pasted on the surface of the SMPC laminate; then, a 230-type film electric heater (Beijing Hongyu Aero-Technology Co., Ltd., China) was applied on the double-sided pressure-sensitive tape. Finally, 3M 92# polyimide film tape was used to wrap the entire SMPC laminate to prevent the film heater from separating from the SMPC laminate. Table S1 in Appendix A lists the data for the 230-type film electric heater used in each component of the SMPC-FDS.

2.3. Experimental section

2.3.1. Quasi-static tensile tests

According to American Society of Testing Materials (ASTM) standard D3039/D3039M, the ESMPC and CSMPC specimens were subjected to quasi-static tensile tests on an MTS809 axial/torsion test system. The geometric dimensions of the two kinds of specimens were 175.0 mm × 25.0 mm × 1.4 mm and 175.0 mm × 25.0 mm × 2.5 mm, respectively. The test system was equipped with an environmental chamber for quasi-static tensile tests at three temperature conditions: −60, 25, and 95 °C, respectively. Prior to loading, the specimens were held at the corresponding temperature for 10 min to allow for uniform heating of the specimens. The quasi-static loading process was achieved by means of displacement control at a constant crosshead speed of 2 mm·min^{-1} until final failure. In addition, tensile tests at 25 °C were performed on specimens exposed to −196 °C (liquid nitrogen) or 95 °C for one month to characterize their low- and high-temperature durability.

2.3.2. Dynamic mechanical analysis (DMA)

DMA tests were performed on SMPC specimens after 3, 6, and 9 months of exposure at −196 °C by means of a dynamic mechanical analyzer (DMA Q800; TA Instrument, USA) to obtain their dynamic thermomechanical properties. All specimens were scanned at a heating rate of 3 °C·min^{-1} in the range of 25–250 °C with a loading frequency of 1 Hz.

2.3.3. Morphology characterization

A scanning electron microscope (SEM; VEGA3 SBH; TESCAN, Czech Republic) was used to characterize the morphology of the specimens before and after tensile fracture. Prior to SEM analysis, the specimens were put into an ETD-800 small ion sputtering instrument for gold plating to improve the image quality.

2.3.4. Shock test

To ensure the safety of the SMPC-FDS under unpredictable shock loads, a pendulum shock-response spectra testing machine

(SP840; Beijing Aerospace Hill Test Technology Co., Ltd., China) was used to perform shock tests on the SMPC-FDS in its folded state under simulated mechanical conditions. The shock test conditions are provided in Table S2 in Appendix A. The shock tests were performed at two temperatures: room temperature (~25 °C) and low temperature (~−60 °C).

2.3.5. Vibration test

The SMPC-FDS underwent a ground launch and multiple reorbits before deployment, and large vibration loads were likely to occur during these processes. In order to verify the resistance of the SMPC-FDS to the vibration environment, the SMPC-FDS was subjected to sinusoidal sweep and random vibration tests by means of an electrodynamic vibration test system. The random vibration test conditions are presented in Table S2.

2.3.6. Thermal vacuum deployment test

The flights of the SMPC-FDS from the Earth–Mars transfer orbit to the Mars remote-sensing orbit occur within a deep cold environment with a high vacuum. To verify the adaptability and deployment performance of the SMPC-FDS in a vacuum environment, vacuum thermal-cycling tests simulating a deep space environment were executed. The simulated deep space thermal-cycling environment was as follows: a vacuum pressure below 10^{-3} Pa, and high- and low-temperature sections at 85 and −145 °C, respectively, for a total of 3.5 cycles of approximately 27 h each. In the last cycle, the locking laminate, releasing laminate, and SMPC hinge were deployed at the three temperatures of −100, −60, and 25 °C with a nominal energization voltage of 29 V. During the thermal vacuum deployment of the components, the temperature changes on the components were monitored by the thermistor (PT100; Shenzhen BD RTD Sensors Technology Co., Ltd., China) attached to each component, and the deployment process of the components was recorded with a camera.

3. Results and discussion

3.1. Mechanical properties of the materials

The reinforced phase of the SMPC is a plain-weave fabric with fibers laid at ±45°, as shown in Fig. 2(a). Unlike unidirectional fibers, the fibers in the plain-weave fabric are arranged in a wavy cross pattern, which effectively increases the elongation of the SMPC when it is subjected to a tensile load. In particular, the elongation of the SMPC is further enhanced when the loading direction does not coincide with the fiber direction. Parts (i) and (iii) of Fig. 2(a) respectively present the macroscopic and microscopic fracture patterns of the SMPC after it is subjected to a tensile load with a loading direction at an angle of 45° to the fiber. In part (iii) of Fig. 2(a), it can be observed that the fracture surface of the fiber bundles is uneven, which implies a progressive failure process. The progressive failure pattern contributes a greater elongation to the SMPC than the brittle fracture pattern often seen in unidirectional fiber-reinforced composites. The tensile stress–strain curves of the ESMPC and CSMPC at −60, 25, and 95 °C are respectively plotted in Figs. 2(b) and (c). The ultimate strength of the ESMPC and CSMPC gradually decreases, but the elongation at the break increases significantly as the temperature increases, which is attributed to the temperature-induced variable stiffness of the SMP matrix. Notably, the increased elongation at the break facilitates the shape programming of the SMPCs at high temperature. A comparison of Figs. 2(b) and (c) show that the ultimate strength of the CSMPC is higher than that of the ESMPC at the same temperature, due to the higher fiber content of the CSMPC and the slightly higher strength of the cyanate-based SMP in comparison with the epoxy-based SMP.

Since the flight of the SMPC-FDS from an Earth–Mars transfer orbit to a Mars orbit occurred in unpredictable high- or low-temperature environments, it was necessary to investigate the effects of long-term high- or low-temperature exposure on the mechanical properties of the SMPCs. The tensile stress–strain curves of the ESMPC and CSMPC at 25 °C after prolonged high- or low-temperature exposure are shown in Fig. 2(d), and statistical data on their tensile strength, tensile modulus, elongation at break, and toughness is presented in Figs. 2(e) and (f). Compared with low-temperature exposure, long-term high-temperature exposure has little effect on the tensile strength and modulus of the ESMPC but enhances those of the CSMPC. However, in terms of elongation at the break and toughness, long-term high-temperature exposure has an insignificant effect on the CSMPC but enhances the ESMPC.

In addition, the molecular structure and thermal stability of the ESMPC and CSMPC before and after high- or low-temperature exposure were evaluated by Fourier-transform infrared spectroscopy (FTIR) analysis and thermogravimetric analysis, respectively. The positions of the characteristic peaks in the FTIR spectra of the SMPCs did not change before and after the SMPCs were subjected to high- or low-temperature exposure, implying that the SMPCs possess a stable molecular structure (Fig. S3 in Appendix A). The thermogravimetric analysis shows that the thermogravimetric curves of the SMPCs before and after high- or low-temperature exposure are in general agreement, which confirms that the high- or low-temperature exposure did not adversely affect the thermal stability (or thermal degradability) of the ESMPC and CSMPC (Fig. S4 in Appendix A).

T_g is a thermodynamic parameter of SMPCs that determines the lower temperature limit at which the SMPCs can be fully deployed. Figs. 2(g) and (h) respectively present the DMA curves of the ESMPC and CSMPC after 3, 6, and 9 months of low-temperature exposure, from which thermodynamic characteristics such as the T_g, storage modulus, and loss tangent (Tanδ) can be obtained. During prolonged low-temperature exposure, a crosslinking reaction occurred between the epoxy (or cyanate) resin and the hardener, which was evidenced by a slight increase in T_g (reflecting the extent of crosslinking density). In fact, the process of low-temperature exposure was similar to stepwise curing, which led to a more complete transition from the resin monomer to the macromolecule; hence, the T_g changed [29]. Nevertheless, the T_g of the ESMPC remained in the range of 120–150 °C, so the deployment reliability of the SMPC hinges was not weakened. The effect of long-term low-temperature exposure on the T_g of the CSMPC was negligible.

3.2. Structural dynamic performance

During the launch and multiple reorbits of Tianwen-1, the SMPC-FDS might suffer from environments with unpredictable shock and vibration; thus, dynamics tests including shock tests, sinusoidal sweep tests, and random vibration tests were needed to evaluate the mechanical reliability of the SMPC-FDS in the folded state. Fig. 3(a) provides an image of the SMPC-FDS used for the structural dynamics tests, in which the three loading directions and the locations of the two acceleration measurement points are marked. Two measurement points are positioned above the releasing laminate and behind the camera to output the response at the lock–release mechanism and the optical camera, respectively. Fig. 3(b) presents the shock-response spectrum of the SMPC-FDS at 25 °C for different loading directions. The black, red, blue, and green curves represent the actual input shock spectrum, the restricted region of the input shock spectrum, and the response spectrum of measurement points 1 and 2, respectively. The response of measurement point 2 is significantly weaker than that of measurement point 1, indicating that the shock load transferred to the camera through the

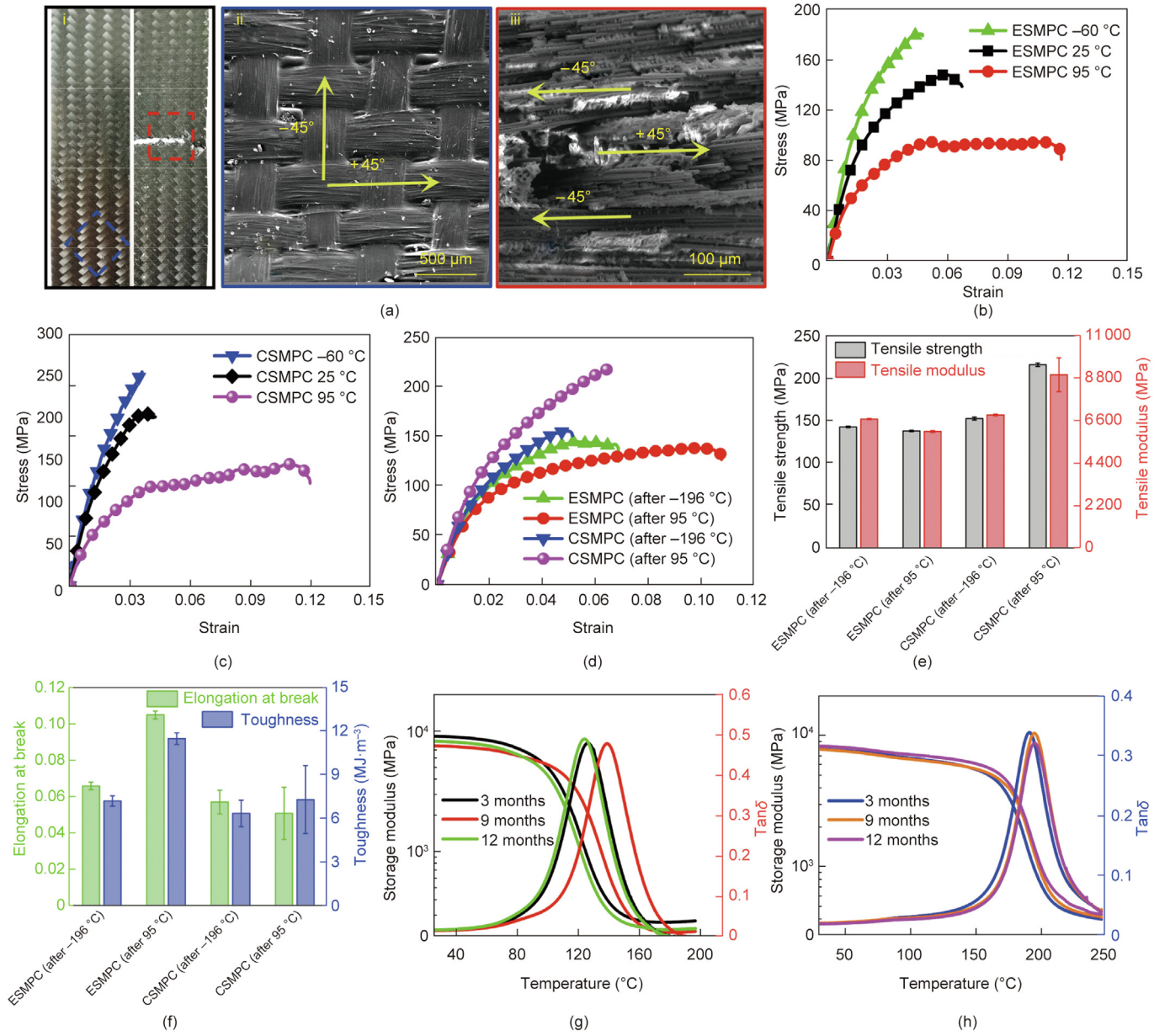

Fig. 2. Temperature-dependent mechanical properties of SMPCs in the SMPC-FDS. (a) Surface morphology of ESMPC laminate before and after tensile fracture: (i) macroscopic morphology of ESMPC laminates before and after fracture; (ii) local surface morphology of plain-weave ESMPC; and (iii) microscopic morphology of ESMPC laminate after tensile fracture. Tensile stress–strain curves of (b) ESMPC and (c) CSMPC at various temperatures. (d) Tensile stress–strain curves, (e) strength/modulus, and (f) elongation at break/toughness of SMPCs at 25 °C after exposure to −196 or 95 °C for one month. DMA curves of (g) ESMPC and (h) CSMPC after experiencing low-temperature exposure.

flexible deployable mechanism has been tremendously attenuated, which is beneficial for the mechanically sensitive optical camera. Fig. 3(c) exhibits the shock spectrum of the SMPC-FDS at −60 °C when loaded in the *X* direction, while the shock spectrum in other directions, such as the *Y* and *Z* directions, are presented in Fig. S5 in Appendix A. It should be noted that the response spectrum of the SMPC-FDS at −60 °C was not measured, because it was difficult to affix the acceleration sensor in the low-temperature environment. Nevertheless, the results indicate that the SMPC-FDS still performs satisfactorily after being subjected to a low-temperature shock at −60 °C.

The fundamental frequency is a key parameter for characterizing the structural dynamic performance. Sinusoidal sweep tests (0.2*g*, where *g* denotes the acceleration of gravity) were conducted to determine the fundamental frequency of the SMPC-FDS. The frequency response curves for measurement points 1 and 2 are presented in Figs. 3(d) and (e), respectively. The frequency response curves obtained from the same measurement points are not consistent when the loading direction is different; in addition, there are differences in the fundamental frequencies obtained from various frequency response curves. The average values of the fundamental frequencies obtained for measurement points 1 and 2 in all directions were 32.5 and 33.3 Hz, respectively, which met the requirements of the Tianwen-1 probe.

The random vibration responses of the SMPC-FDS in the *X* and *Z* directions are depicted in Figs. 3(f) and (g), respectively, while the responses in the *Y* direction are presented in Fig. S5. From these random vibration-response curves, it can be observed that the response of measurement points 1 and 2 gradually weakens compared with the input. The acceleration root mean square (RMS) is

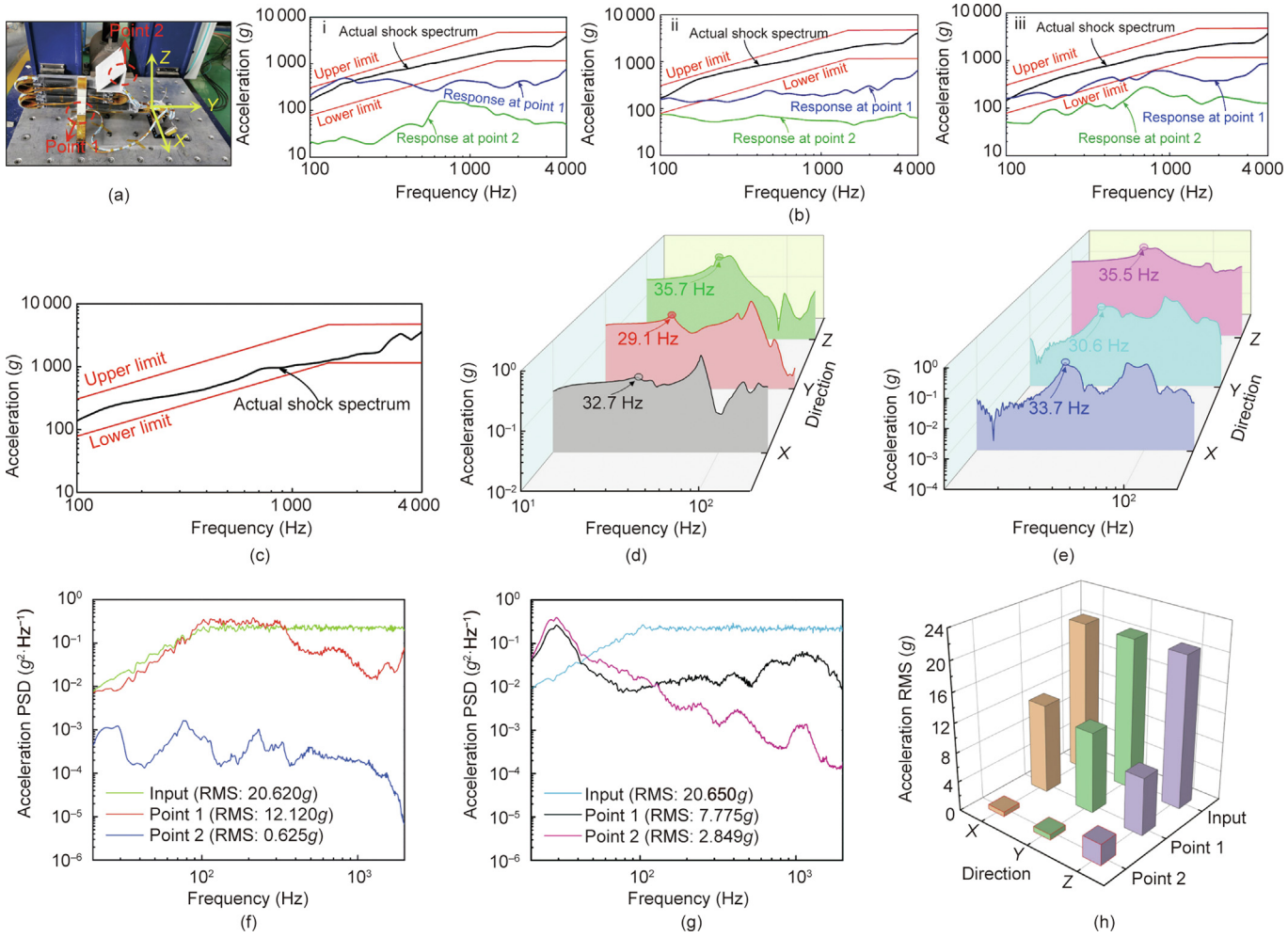

Fig. 3. Structural dynamics performance of the SMPC-FDS. (a) The SMPC-FDS used for structural dynamics testing. (b) Shock-response spectrum of the SMPC-FDS at 25 °C: (i) *X* direction; (ii) *Y* direction; and (iii) *Z* direction. (c) Shock spectrum of the SMPC-FDS loaded in the *X* direction at −60 °C. Frequency response curves of (d) point 1 and (e) point 2 at a sinusoidal sweep of 0.2*g* (where *g* denotes the acceleration of gravity). Frequency response curves of the SMPC-FDS when performing random vibration in the (f) *X* direction and (g) *Z* direction. (h) Acceleration root mean square (RMS) of the frequency response curves of the SMPC-FDS when random vibration is executed in each direction. PSD: power spectral density.

an indicator for measuring random vibration. Fig. 3(h) lists the acceleration RMS versus the input value for each measurement point of the SMPC-FDS. The acceleration RMS at measurement points 1 and 2 is respectively attenuated by 41.2% and 97.0% from the input when loaded in the *X* direction, while the corresponding attenuation values are 62.3% and 86.2% when loaded in the *Z* direction.

3.3. Thermal vacuum deployment reliability

Thermal vacuum cycling testing of the SMPC-FDS and thermal vacuum deployment testing of the SMPC components after cycling were carried out by simulating the deep space environment. Figs. 4(a) and (b) present photographs of the SMPC-FDS and its components, respectively, during the thermal vacuum tests. Thermistors were attached to the SMPC components to monitor the temperature variations in real time during deployment. Figs. 4(c) and (d) respectively show the temperature history and vacuum pressure curve during the thermal vacuum cycle test. Thermal vacuum deployment tests of various components, including the SMPC hinges, releasing laminates, and locking laminates, were performed at −100, −60, and 25 °C during the last temperature cycle; the temperature variations of the components during deployment are shown in Figs. 4(e)–(g). The results indicate that the lower the ambient temperature is, the lower the temperature of the SMPC component will be for the same energizing time. When the SMPC hinge, releasing laminate, and locking laminate were energized at 29 V for 120 s in a vacuum environment at −60 °C, their temperatures were 141, 198, and 200 °C, respectively, which were higher than the T_g of the corresponding materials. Fig. S6 in Appendix A illustrates the deployment process of the SMPC hinge in a vacuum environment at different temperatures, from which it can be seen that the time required for full deployment of the hinge varies with the ambient temperature. The thermal vacuum deployment processes of the releasing laminate and locking laminate are also depicted (Fig. S7 in Appendix A). The time required for the full deployment of various components as a function of temperature is plotted in Fig. S8 in Appendix A, from which it can be concluded that the deployment time increases as the temperature decreases.

3.4. On-orbit functional identification

After the long-term deep space flight phases such as the Earth–Mars transfer phase and the Mars mooring phase, the SMPC-FDS arrived in a Mars remote-sensing orbit with Tianwen-1, where its

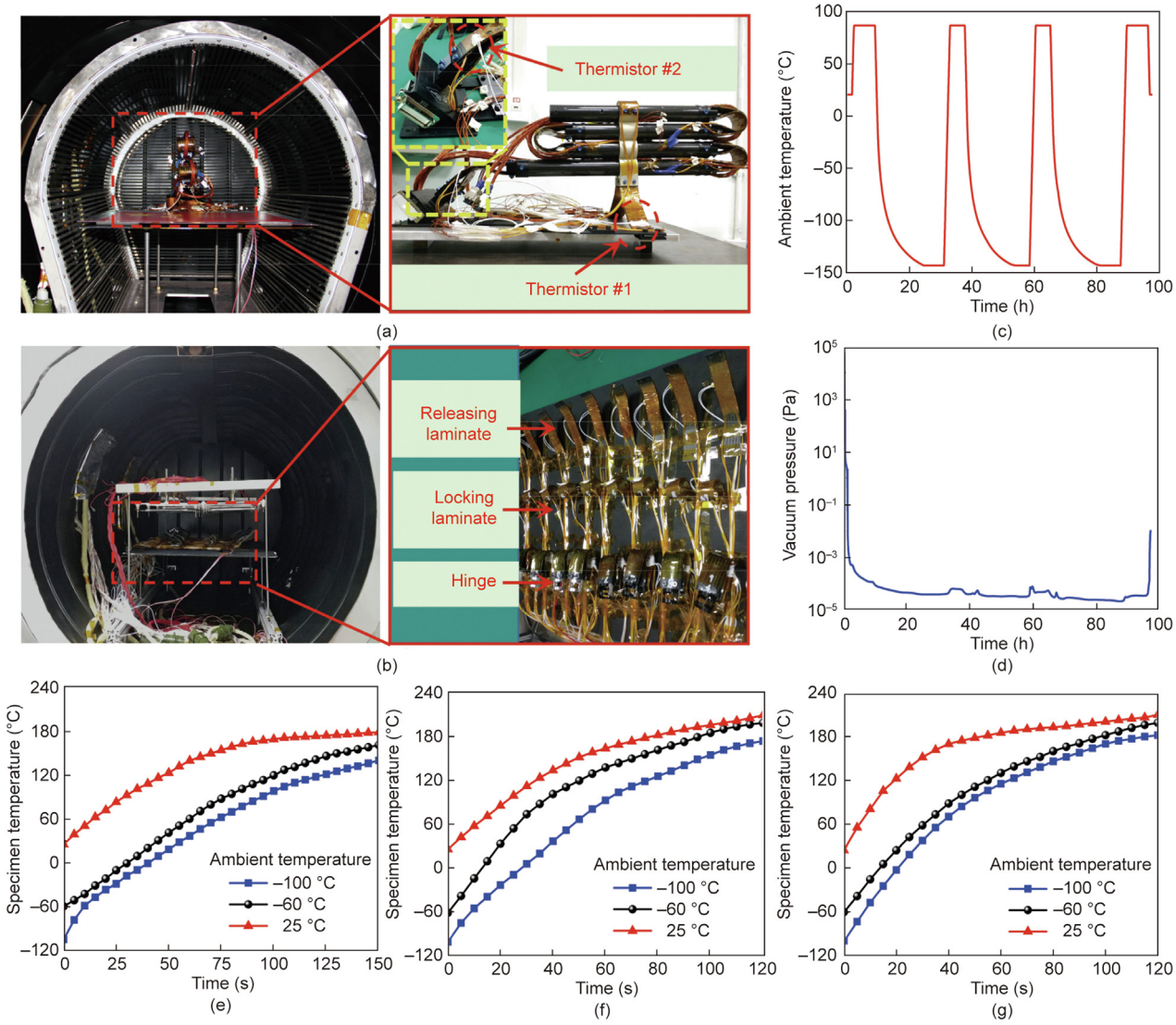

Fig. 4. Deployment tests of the SMPC-FDS in a simulated thermal vacuum environment. (a) The SMPC-FDS and (b) various components during the thermal vacuum test; (c) temperature history and (d) ambient pressure profile during the thermal vacuum test; temperature–time profiles of (e) SMPC hinges, (f) releasing laminates, and (g) locking laminates during thermal vacuum deployment.

on-orbit deployment was demonstrated. The states of the SMPC-FDS before and after its deployment during the ground test are respectively shown in Figs. 5(a) and (b), and are consistent with the states before and after its on-orbit deployment. The on-orbit deployment demonstration of the SMPC-FDS was accomplished by sending energization commands from Earth to the Tianwen-1 probe in the Mars orbit. Following the deployment sequence of the SMPC-FDS presented in Fig. S1, a total of six commands were sent to power the locking laminate, releasing laminate 1/2, first, second, third, and fourth hinge, respectively. The energization voltage and energization time for each component are listed in Table S3 in Appendix A.

Fig. 5(c) presents the environment temperature around the orbiter before and after the on-orbit energized deployment of the SMPC-FDS, as fed back by the temperature telemetry points. The temperatures obtained from telemetry points 1 and 2 before the SMPC-FDS deployment were −39 and −7 °C, respectively; the difference between these two temperatures is attributed to the difference in the sun exposure and heat dissipation caused by the different positions of the telemetry points. Since the two temperature telemetry points are located on the releasing laminate and first hinge, respectively, they were also able to provide feedback on the temperature changes of the releasing laminate and first hinge during the on-orbit energized deployment of the SMPC-FDS. As shown in Fig. 5(c), the maximum temperatures of the two components during the energized deployment were 204 and 123 °C, respectively. After the energization was terminated, the temperature of each component decayed nearly exponentially to the environment temperature.

During the deployment of the SMPC-FDS, the camera carried at its end was able to capture the attitude of the Tianwen-1 orbiter from different angles. Fig. 5(d) shows how the camera's field of view changed during the SMPC-FDS deployment. When fully deployed, the camera was able to shoot the national flag of China fixed on the orbiter from the front. Fig. 5(e) presents the brightly colored flag captured by the camera on the SMPC-FDS in the Mars orbit just as the Tianwen-1 orbiter flew over the Martian North Pole. In addition, the camera on the SMPC-FDS was able to monitor the change in the solar illumination angle during the attitude adjustment of the Tianwen-1 orbiter.

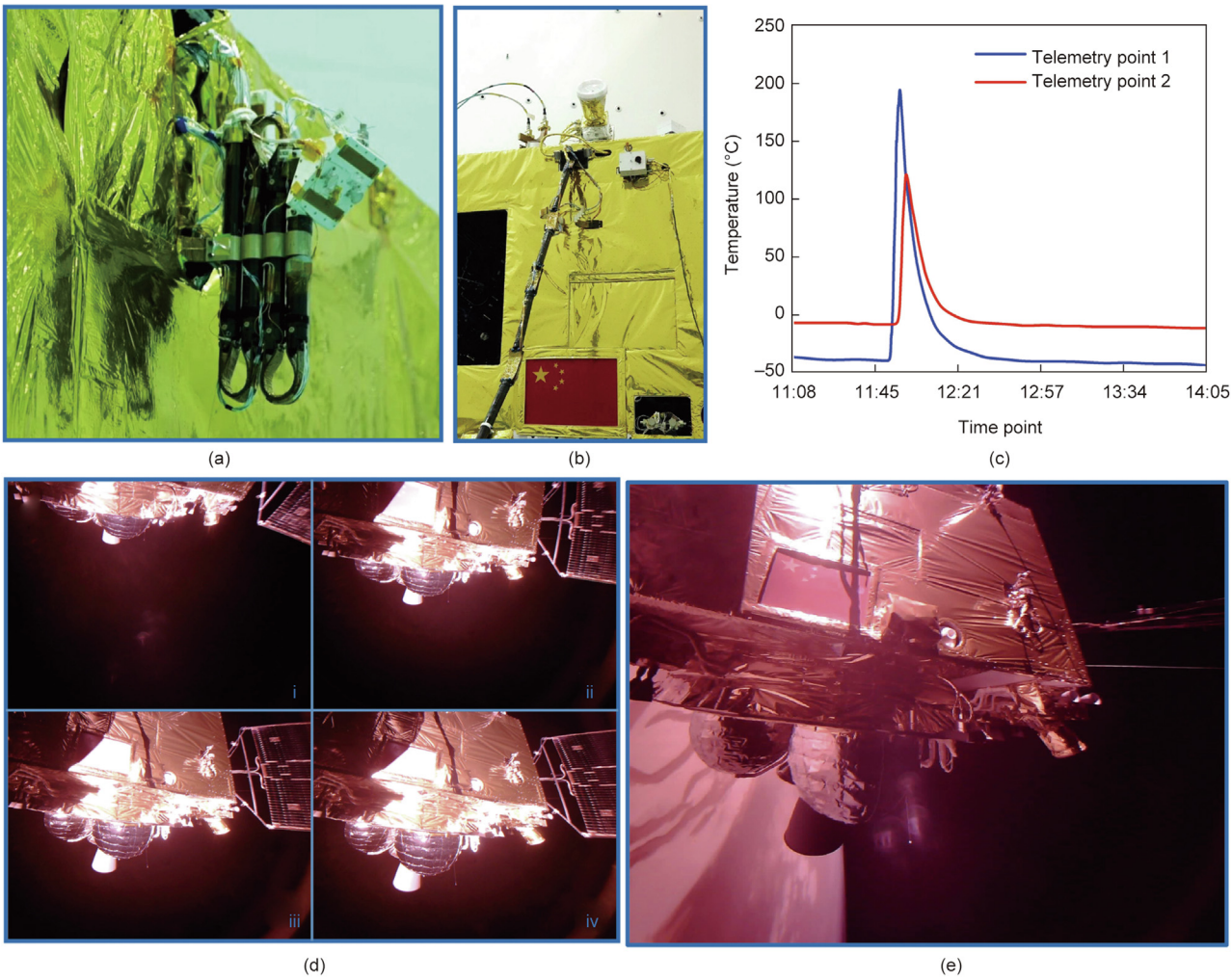

Fig. 5. Functional identification of the SMPC-FDS. (a) Folded state of the SMPC-FDS during the ground test phase; (b) deployed state of the SMPC-FDS during the ground test phase; (c) temperature telemetry before and after on-orbit deployment; (d) field-of-view change process of the camera on the SMPC-FDS during on-orbit deployment; (e) the national flag of China captured by the camera on the SMPC-FDS after on-orbit deployment.

4. Conclusions

A flexible deployable subsystem termed the SMPC-FDS was proposed for the Tianwen-1 Mars exploration mission and was deployed in a Mars orbit. The temperature telemetry points and monitoring camera arranged on the SMPC-FDS were respectively capable of monitoring the environment around Tianwen-1 and photographing the local state of the orbiter. The SMPC-FDS consists of a lock–release mechanism and a multi-stage deployable mechanism in which the functional materials are thermotropic SMPCs that can deploy under certain temperature conditions. A series of characterization methods were applied to confirm the adequate thermomechanical properties and space-environment adaptability of the SMPCs. Mechanical shock and vibration tests were performed to simulate the harsh mechanical environment during the ground launch phase and deep space flight phase, and the results showed that the SMPC-FDS possessed satisfactory resistance to the mechanical environment. To demonstrate the deployment reliability of the SMPC-FDS in a Mars orbit, the deployment performance of each component in the SMPC-FDS was evaluated in a simulated thermal vacuum environment. The power-on times for each component at different temperatures were obtained from the thermal vacuum deployment tests; then, the power-on time of each component for on-orbit deployment was determined from the temperature data returned by the temperature telemetry points on the SMPC-FDS.

On 23 July 2020, the SMPC-FDS was successfully launched together with the Tianwen-1 Mars probe. After nearly 16 months of deep space flight, the SMPC-FDS completed its deployment demonstration in a Mars orbit on 11 November 2021. After the SMPC-FDS was launched from the ground, the temperature telemetry points on the SMPC-FDS continuously monitored the temperature environment around the Tianwen-1 probe and transmitted a wealth of scientific data back to Earth. Moreover, after the deployment of the SMPC-FDS, the large field-of-view camera carried on it was able to steadily capture local details of the orbiter and successfully photographed the national flag of China that was fixed on the orbiter. The successful qualification of the SMPCs in the Mars exploration project presented in this study is a milestone in the field of aerospace engineering, as it marks the application of smart materials and fiber-reinforced composites in deep space exploration.

Acknowledgments

The authors would like to thank all members of the Smart Material and Structure Group at the Harbin Institute of Technology and

the Shanghai Institute of Satellite Engineering. This work is supported by the National Natural Science Foundation of China (11632005) and the Heilongjiang Touyan Innovation Team Program.

Compliance with ethics guidelines

Chengjun Zeng, Liwu Liu, Yang Du, Miao Yu, Xiaozhou Xin, Tianzhen Liu, Peilei Xu, Yu Yan, Dou Zhang, Wenxu Dai, Xin Lan, Fenghua Zhang, Linlin Wang, Xue Wan, Wenfeng Bian, Yanju Liu, and Jinsong Leng declare that they have no conflict of interest or financial conflicts to disclose.

Appendix A. Supplementary data

Supplementary data to this article can be found online at https://doi.org/10.1016/j.eng.2023.01.005.

References

[1] Chen Q, Sun D. Condensation heat transfer enhancement mechanism for vertical upflows by the phase separation concept at small gravity. Sci Bull 2015;60(20):1759–67.
[2] Chandra M, Kumar S, Chattopadhyaya S, Chatterjee S, Kumar P. A review on developments of deployable membrane-based reflector antennas. Adv Space Res 2021;68(9):3749–64.
[3] Yang S, Sultan C. Modeling of tensegrity-membrane systems. Int J Solids Struct 2016;82:125–43.
[4] Wang D, Ma J, Li P, Fan L, Wu Y, Zhang Z, et al. Flexible hard coatings with self-evolution behavior in a low earth orbit environment. ACS Appl Mater Interfaces 2021;13(38):46003–14.
[5] Buckner TL, Bilodeau RA, Kim SY, Kramer-Bottiglio R. Roboticizing fabric by integrating functional fibers. Proc Natl Acad Sci USA 2020;117(41):25360–9.
[6] Al-Mansoori M, Khan KA, Cantwell WJ. Harnessing architected stiffeners to manufacture origami-inspired foldable composite structures. Compos Sci Technol 2020;200:108449.
[7] Daynes S, Grisdale A, Seddon A, Trask R. Morphing structures using soft polymers for active deployment. Smart Mater Struct 2014;23(1):012001.
[8] Sealy C. Molecular nanostructures make high-energy shape memory polymers. Nano Today 2021;41:101321.
[9] Mattmann M, De Marco C, Briatico F, Tagliabue S, Colusso A, Chen XZ, et al. Thermoset shape memory polymer variable stiffness 4D robotic catheters. Adv Sci 2022;9(1):2103277.
[10] Zeng C, Liu L, Hu Y, Bian W, Leng J, Liu Y. A viscoelastic constitutive model for shape memory polymer composites: micromechanical modeling, numerical implementation and application in 4D printing. Mech Mater 2022;169:104301.
[11] Zeng C, Liu L, Bian W, Leng J, Liu Y. Compression behavior and energy absorption of 3D printed continuous fiber reinforced composite honeycomb structures with shape memory effects. Addit Manuf 2021;38:101842.
[12] Zhao F, Zheng X, Zhou S, Zhou B, Xue S, Zhang Y. Constitutive model for epoxy shape memory polymer with regulable phase transition temperature. Int J Smart Nano Mater 2021;12(1):72–87.
[13] Zhang F, Wen N, Wang L, Bai Y, Leng J. Design of 4D printed shape-changing tracheal stent and remote controlling actuation. Int J Smart Nano Mater 2021;12(4):375–89.
[14] Momeni F, Ni J. Laws of 4D printing. Engineering 2020;6(9):1035–55.
[15] Xia Y, He Y, Zhang F, Liu Y, Leng J. A review of shape memory polymers and composites: mechanisms, materials, and applications. Adv Mater 2021;33(6):2000713.
[16] Gu J, Zhang X, Duan H, Wan M, Sun H. A hygro–thermo–mechanical constitutive model for shape memory polymers filled with nano-carbon powder. Int J Smart Nano Mater 2021;12(3):286–306.
[17] Jarali CS, Madhusudan M, Vidyashankar S, Raja S. A new micromechanics approach to the application of Eshelby's equivalent inclusion method in three phase composites with shape memory polymer matrix. Compos Part B Eng 2018;152:17–30.
[18] Liu T, Liu L, Yu M, Li Q, Zeng C, Lan X, et al. Integrative hinge based on shape memory polymer composites: material, design, properties and application. Compos Struct 2018;206:164–76.
[19] Roh JH, Bae JS. Softenable composite boom for reconfigurable and self-deployable structures. Mech Adv Mater Struct 2017;24(8):698–711.
[20] Liu Y, Du H, Liu L, Leng J. Shape memory polymers and their composites in aerospace applications: a review. Smart Mater Struct 2014;23(2):023001.
[21] Liu Z, Lan X, Bian W, Liu L, Li Q, Liu Y, et al. Design, material properties and performances of a smart hinge based on shape memory polymer composites. Compos Part B Eng 2020;193:108056.
[22] Li F, Liu L, Lan X, Wang T, Li X, Chen F, et al. Modal analyses of deployable truss structures based on shape memory polymer composites. Int J Appl Mech 2016;8(7):1640009.
[23] Li F, Liu L, Lan X, Pan C, Liu Y, Leng J, et al. Ground and geostationary orbital qualification of a sunlight-stimulated substrate based on shape memory polymer composite. Smart Mater Struct 2019;28(7):075023.
[24] Lan X, Liu L, Zhang F, Liu ZX, Wang LL, Li QF, et al. World's first spaceflight on-orbit demonstration of a flexible solar array system based on shape memory polymer composites. Sci China Technol Sci 2020;63(8):1436–51.
[25] Yan W, Liu J, Ren X, Li C, Fu Q, Wang D, et al. Detection capability verification and performance test for the high resolution imaging camera of China's Tianwen-1 mission. Space Sci Rev 2021;217(6):71.
[26] Zhao W. Tianwen-1 and China's Mars exploration program. Natl Sci Rev 2021;8(2):nwaa285.
[27] Zou Y, Zhu Y, Bai Y, Wang L, Jia Y, Shen W, et al. Scientific objectives and payloads of Tianwen-1, China's first Mars exploration mission. Adv Space Res 2021;67(2):812–23.
[28] Li C, Zhang R, Yu D, Dong G, Liu J, Geng Y, et al. China's Mars exploration mission and science investigation. Space Sci Rev 2021;217(4):57.
[29] Wan X, He Y, Leng J. Investigation of the long-term storage stability of shape memory epoxy prepolymer. Adv Eng Mater 2022;24(4):2101023.
[30] Wang L, Zhang F, Liu Y, Du S, Leng J. Thermal, mechanical and shape fixity behaviors of shape memory cyanate under γ-ray radiation. Smart Mater Struct 2022;31(4):045010.
[31] Xie F, Gong X, Huang L, Liu L, Leng J, Liu Y. Effects of accelerated aging on thermal, mechanical, and shape memory properties of a cyanate-based shape memory polymer: II atomic oxygen. Polym Degrad Stabil 2021;186:109515.
[32] Liu Z, Li Q, Bian W, Lan X, Liu Y, Leng J. Preliminary test and analysis of an ultralight lenticular tube based on shape memory polymer composites. Compos Struct 2019;223:110936.